Rapid Communications

Nodal multigap superconductivity in $KCa_2Fe_4As_4F_2$

M. Smidman,[1,*] F. K. K. Kirschner,[2] D. T. Adroja,[3,4,†] A. D. Hillier,[3] F. Lang,[2] Z. C. Wang,[5] G. H. Cao,[5] and S. J. Blundell[2]

[1]*Center for Correlated Matter and Department of Physics, Zhejiang University, Hangzhou 310058, China*

[2]*Department of Physics, University of Oxford, Clarendon Laboratory, Parks Road, Oxford OX1 3PU, United Kingdom*

[3]*ISIS Facility, Rutherford Appleton Laboratory, Chilton, Didcot Oxon, OX11 0QX, United Kingdom*

[4]*Highly Correlated Matter Research Group, Physics Department, University of Johannesburg, PO Box 524, Auckland Park 2006, South Africa*

[5]*Department of Physics, Zhejiang University, Hangzhou 310027, China*

(Received 30 November 2017; published 22 February 2018)

We find evidence that the newly discovered Fe-based superconductor $KCa_2Fe_4As_4F_2$ ($T_c = 33.36(7)$ K) displays multigap superconductivity with line nodes. Transverse field muon spin rotation (μSR) measurements show that the temperature dependence of the superfluid density does not have the expected behavior of a fully gapped superconductor, due to the lack of saturation at low temperatures. Moreover, the data cannot be well fitted using either single band models or a multiband s-wave model, yet are well described by two-gap models with line nodes on either one or both of the gaps. Meanwhile the zero-field μSR results indicate a lack of time reversal symmetry breaking in the superconducting state, but suggest the presence of magnetic fluctuations. These results demonstrate a different route for realizing nodal superconductivity in iron-based superconductors. Here the gap structure is drastically altered upon replacing one of the spacer layers, indicating the need to understand how the pairing state is tuned by changes of the asymmetry between the pnictogens located either side of the Fe planes.

DOI: 10.1103/PhysRevB.97.060509

Following the discovery of the second family of high temperature superconductors, the iron pnictides [1,2], there has been considerable effort to understand the underlying mechanism for the formation of Cooper pairs. Identifying the pairing symmetry is one of the most important means of determining the mechanism, for which it is vital to characterize the superconducting gap structure [3]. Many iron-arsenide-based superconductors have been proposed to have $s_\pm$ pairing symmetry where the superconductivity is mediated by spin fluctuations [4,5]. Here the superconducting gap remains fully open across the whole Fermi surface, but there is a change of sign of the gap between the hole pockets at the Brillouin zone center and the electron pockets at the zone edge. This scenario is well supported by measurements of the gap symmetry of many compounds, where evidence for two-gap nodeless superconductivity is found [6–13].

However, the universality of this picture was called into question by the observation of nodal superconductivity in a number of FeAs-based superconductors. These include the 1111 oxypnictides [14–16], $BaFe_2(As_{1-x}P_x)$ [17–20], and KFe_2As_2 [21–25]. The latter material corresponds to the heavily hole doped region of the phase diagram with a relatively low superconducting transition temperature of $T_c \approx 3$ K, as compared to the optimally doped $Ba_{0.6}K_{0.4}Fe_2As_2$ which has a higher value of $T_c \approx 37$ K and two nodeless gaps [6]. This crossover from nodeless to nodal superconductivity was suggested to correspond to a change from $s_\pm$ to d-wave pairing symmetry [25–27]. Between these states the system would be expected to pass through a time reversal symmetry breaking $s + id$ state [28]. Mixed evidence for such a phase has been found from muon-spin relaxation (μSR), where time reversal symmetry breaking was not found in initial measurements [29], but evidence was subsequently observed from measurements of ion-irradiated samples [30]. Meanwhile ARPES measurements indicate that KFe_2As_2 displays nodal superconductivity but with an s-wave pairing state overall [24].

The "122" structure of $(Ba,K)Fe_2As_2$ is body centered tetragonal, where the Fe_2As_2 layers which are ubiquitous in the iron arsenide superconductors, are situated between layers of the alkaline/alkaline earth atoms. However, FeAs-based materials consisting of different layered arrangements can also be synthesized such as $CaAFe_4As_4$ (A = K, Rb, Cs) [31]. In this case, the structure now has alternating sheets of Ca and A atoms along the c axis, which breaks the symmetry in the Fe_2As_2 layers and the As atoms above and below the Fe plane are no longer crystallographically equivalent. Meanwhile stoichiometric $CaKFe_4As_4$ has a high T_c of around 35 K, and is intrinsically near optimal hole doping [31,32]. Measurements of the superconducting gap structure and inelastic neutron scattering give clear evidence for a nodeless $s_\pm$ pairing state, in line with the optimally doped "122" materials [12,13,33–35].

Another recently discovered variant showing high temperature superconductivity are $ACa_2Fe_4As_4F_2$ (A = K, Rb, Cs) [36,37]. The crystal structure is displayed in Fig. 1(a), where the Fe_2As_2 layers are now surrounded by A atoms on one side and Ca_2F_2 on the other, again leading to two distinct As sites above and below the Fe plane. These materials also show large T_c values of 28–33 K, depending on the element A, and are situated near optimal doping. However the nature of the superconducting gap and therefore the pairing states of these new variants have not been characterized. In this Rapid Communication we report zero and transverse field

*msmidman@zju.edu.cn

†devashibhai.adroja@stfc.ac.uk

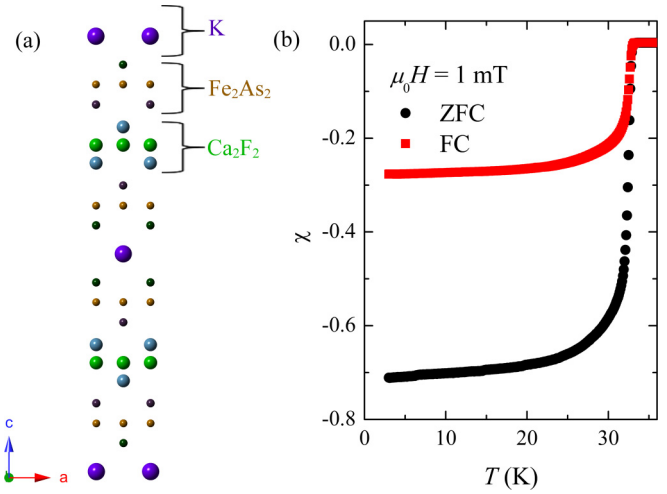

FIG. 1. (a) Crystal structure of $KCa_2Fe_4As_4F_2$, where the K (purple), Fe (brown), As (dark green), Ca (blue), and F (light green) atoms are displayed. The structure consists of Fe_2As_2 layers which lie between K atoms on one side and Ca_2F_2 on the other. (b) Temperature dependence of the magnetic susceptibility of $KCa_2Fe_4As_4F_2$ for both zero-field cooled (ZFC) and field-cooled (FC) measurements.

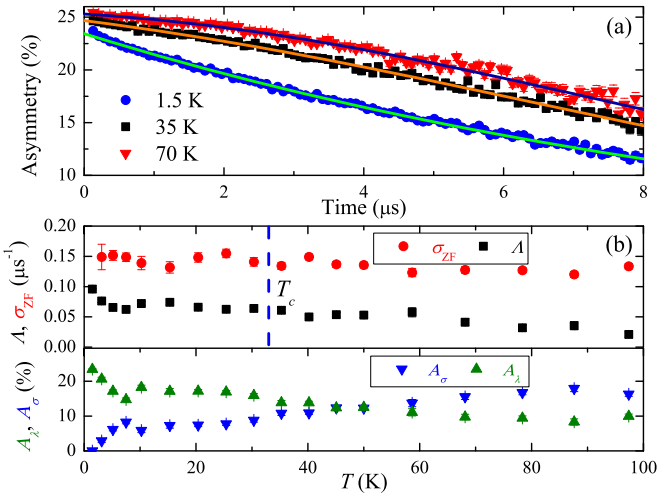

FIG. 2. (a) Zero-field μSR spectra at three temperatures, where the solid lines show fits to the data described in the text. (b) Temperature dependence of the Lorentzian (Λ) and Gaussian (σ_{ZF}) relaxation rates, along with the corresponding amplitudes of each component, from fits to the zero-field μSR.

μSR measurements of $KCa_2Fe_4As_4F_2$. The superfluid density derived from the depolarization rate of the transverse field measurements shows a lack of saturation at low temperatures, and the analysis provides clear evidence for nodal multigap superconductivity. Meanwhile, the relaxation observed in zero-field μSR shows a weak temperature dependence but no evidence for time reversal symmetry breaking upon entering the superconducting state. These results indicate a different route to nodal superconductivity in high temperature FeAs-based superconductors.

Polycrystalline samples of $KCa_2Fe_4As_4F_2$ were synthesized using the solid state reaction method described in Ref. [36]. As can be seen from the temperature dependence of the magnetic susceptibility shown in Fig. 1(b), the samples show a sharp superconducting transition at around $T_c \approx 33$ K. Muon-spin relaxation/rotation (μSR) measurements were performed on the MuSR spectrometer at the ISIS facility [38]. Spin-polarized positive muons are implanted into the sample, which decay with a half-life of 2.2 μs, emitting a positron. Since the positrons are preferentially emitted along the direction of the muon spin, by detecting the asymmetry of the emitted positrons, information can be obtained about the local magnetic field distribution at the muon stopping site. Zero-field μSR measurements were performed with the detectors in the longitudinal configuration, where the stray magnetic fields are canceled to within 1 μT using an active compensation system. The transverse field measurements were performed with detectors in a transverse arrangement, with a field of 40 mT applied perpendicular to the initial muon polarization direction. The $KCa_2Fe_4As_4F_2$ sample was powdered and mounted on a silver plate (99.999%), since the signal from muons stopping in silver depolarizes at a negligible rate. All of the data were analyzed using WiMDA [39].

Zero-field μSR measurements were performed from 1.5 to 100 K, and the observed asymmetries are displayed in Fig. 2(a) for three temperatures. The data were fitted with the sum of a Lorentzian and Gaussian relaxation function $A(t) = A_\lambda \exp(-\Lambda t) + A_\sigma \exp(-\sigma_{ZF}^2 t^2/2) + A_{bg}$, where the background term A_{bg} was fixed from fitting at 100 K. It should also be noted that at 1.5 K, there is evidence for a small additional fast relaxation at short times. The fitted parameters are displayed in Fig. 2(b), where it can be seen that with decreasing temperature, there is a gradual increase of Λ, whereas there is little change of σ_{ZF}. These results suggest the presence of weak magnetic fluctuations, but neither quantity shows a detectable anomaly upon passing through T_c, indicating an absence of time reversal symmetry breaking. However, since $\Lambda(T)$ is not temperature independent, a small time reversal symmetry breaking signal as observed in some superconductors cannot be completely excluded [40,41].

Figures 3(a) and 3(c) display μSR spectra measured in a transverse field of 40 mT, performed at 40 K and 0.3 K, respectively, above and below T_c. At 40 K, the muons precess at a single frequency, as shown by the maximum entropy spectrum in Fig. 3(b), with a slow depolarization arising from nuclear moments which are quasistatic on the time scale of the muon lifetime. Meanwhile in the superconducting state at 0.3 K, it can be seen that there is a significant increase of the depolarization rate [Fig. 3(c)]. The maximum entropy spectrum in Fig. 3(d) shows that in addition to a sharp narrow peak in the field distribution centered around the applied field, there is also a broader component, the bulk of which corresponds to fields smaller than the applied transverse field. Such a distribution is a clear signature of a type-II superconductor in the mixed state [42].

As shown by the dashed line in Fig. 3(d), the field distribution in the superconducting state can be well accounted for by fitting with two Gaussian functions. Since the narrow component at the applied field corresponds to muons stopping in the silver sample holder, this demonstrates that the field distribution within the vortex lattice is well characterized by a

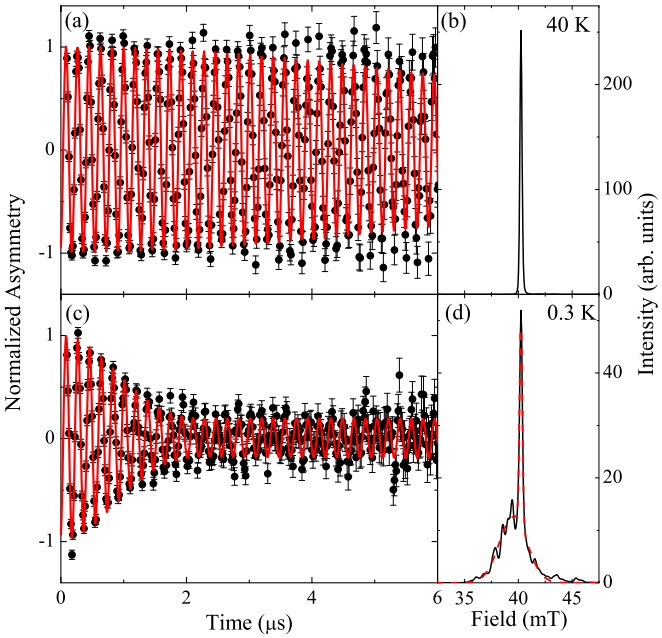

FIG. 3. Muon spin rotation (μSR) measurements of $KCa_2Fe_4As_4F_2$ in a transverse field of 40 mT at (a) 40 K, where (b) displays the maximum entropy spectrum, and (c) at 0.3 K, with the corresponding maximum entropy plot shown in (d). The solid red lines in (a) and (c) show the fits described in the text, while the dashed line in (d) displays a fit with two Gaussian functions.

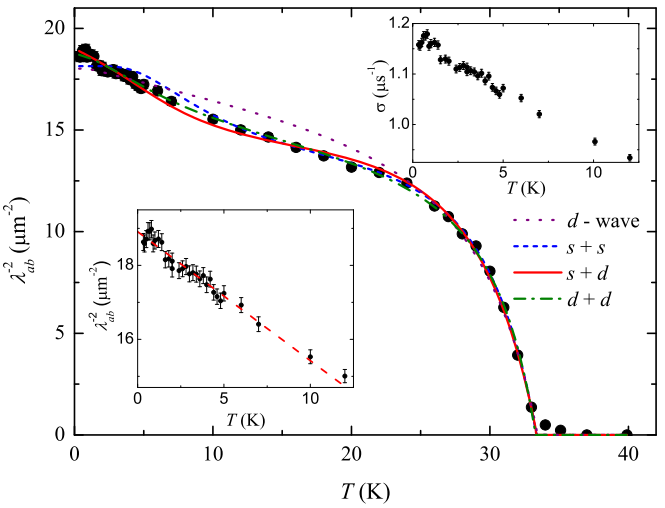

FIG. 4. Temperature dependence of the square of the inverse in-plane penetration depth $\lambda_{ab}^{-2}(T)$, which is proportional to the superfluid density. Fits to different models of the superconducting gap are displayed, where the single gap d-wave and fully gapped $s+s$ models cannot account for the data, while good fits are obtained for the two-gap nodal $s+d$ and $d+d$ models. The insets shows the low temperature behavior of both $\lambda_{ab}^{-2}(T)$ and the total Gaussian relaxation rate σ, where the $\lambda_{ab}^{-2}(T)$ data up to 10 K is consistent with a linear temperature dependence.

single Gaussian centered at a field below 40 mT. Consequently, the time spectra were fitted using

$$A(t) = A_0 e^{-\sigma^2 t^2/2}\cos(\gamma_\mu B_0 t + \phi) + A_1\cos(\gamma_\mu B_1 t + \phi), \quad (1)$$

where $\gamma_\mu/2\pi = 135.5$ MHz/T is the muon gyromagnetic ratio, σ is the Gaussian relaxation rate, ϕ is related to the detector geometry, A_0 and A_1 are the amplitudes of the components from the sample and silver, respectively, while B_0 and B_1 are the corresponding internal magnetic fields. The total amplitudes for each group of detectors were fixed, as well as the amplitude ratio $A_0/A_1 = 4.12$, allowing for the temperature dependence of the muon relaxation rate $\sigma(T)$ to be obtained. We note that adding an additional Gaussian term to Eq. (1) leads to overfitting of the data, and therefore this was not used. In addition, unlike the zero-field measurements, the transverse field spectra are well described at all temperatures by a purely Gaussian relaxation, with no Lorentzian component. The superconducting contribution to the depolarization rate was calculated by subtracting the nuclear contribution via $\sigma_{sc} = \sqrt{\sigma^2 - \sigma_{\rm nuc}^2}$, where the component from the nuclear spins $\sigma_{\rm nuc} = 0.092(1)\,\mu{\rm s}^{-1}$ was determined from the values above T_c. For applied fields much less than the upper critical field, σ_{sc} can be related to the effective penetration depth $\lambda_{\rm eff}$ using $\sigma_{sc}/\gamma_\mu = 0.0609\Phi_0/\lambda_{\rm eff}^2$, where Φ_0 is the magnetic flux quantum [43]. Since the material is an anisotropic layered compound where the out of plane penetration depth (λ_c) greatly exceeds the in-plane value (λ_{ab}), for a polycrystalline sample $\lambda_{\rm eff}$ is dominated by λ_{ab}, where $\lambda_{\rm eff} = 3^{\frac{1}{4}}\lambda_{ab}$ [44].

Figure 4 displays the temperature dependence of $\lambda_{ab}^{-2}(T)$, which is proportional to the superfluid density and therefore provides information about the superconducting gap structure. It can be seen that with decreasing temperature there is no evidence for the saturation of $\lambda_{ab}^{-2}(T)$ down to the lowest measured temperatures, indicating the presence of nodes in the superconducting gap. For a fully gapped superconductor at sufficiently low temperatures, thermal excitations are unable to depopulate the superconducting condensate, leading to constant $\lambda_{ab}^{-2}(T)$. Meanwhile if there are nodes in the gap, there are always low energy excitations comparable to the thermal energy and hence $\lambda_{ab}^{-2}(T)$ will continue to increase upon lowering the temperature. Furthermore, if the gap contains lines of nodes, at low temperatures the temperature dependence of the penetration depth is linear. Therefore for sufficiently low temperatures $\lambda_{ab}^{-2}(T) \approx \lambda_{ab}^{-2}(0) - aT$, where a is a constant, and it can be seen in the inset that the data are compatible with a linear increase from the lowest measured temperature up to around 10 K [corresponding to a total change in $\sigma(T)$ of $\approx 0.2\,\mu{\rm s}^{-1}$].

The normalized superfluid density $\tilde{n}(T) = [\lambda_{ab}(T)/\lambda_{ab}(0)]^{-2}$ was modeled using [45]

$$\tilde{n}(T) = 1 + \frac{1}{\pi}\int_0^{2\pi}\int_{\Delta(T,\varphi)}^{\infty}\frac{\partial f}{\partial E}\frac{E\,dE\,d\varphi}{\sqrt{E^2 - \Delta^2(T,\varphi)}}, \quad (2)$$

where $f = [1 + \exp(-E/k_{\rm B}T)]^{-1}$ is the Fermi-Dirac function. The gap function $\Delta(T,\varphi) = \Delta(T)g(\varphi)$ has a temperature dependence given by $\Delta(T) = \Delta(0)\tanh[(1.82)(1.018(T_c/T - 1))^{0.51}]$ [46], where $\Delta(0)$ is the zero temperature magnitude. The angular dependence $g(\varphi)$ is given by $g(\varphi) = 1$ or $\cos(2\varphi)$ for an s-wave (Δ^s) or d-wave (Δ^d) gap, respectively, (φ = azimuthal angle).

The data were fitted with various models for the superfluid density, with both one and two gaps. Neither a single fully gapped s-wave model (not displayed), nor a single d-wave gap with line nodes can fit the data well. In particular, it can be seen in Fig. 4 that upon reducing the temperature, there is an inflection point at around 10 K, below which there is an upturn in $\lambda_{ab}^{-2}(T)$. Such behavior is difficult to account for with single gap models, but suggests the presence of multiple gaps. Various two-gap models were fitted to the data by adding the weighted sum of two components, where $\tilde{n}(T) = x\tilde{n}_1^{s,d}(T) + (1-x)\tilde{n}_2^{s,d}(T)$, where $\tilde{n}_i^s(\tilde{n}_i^d)$ is the superfluid density corresponding to a gap Δ_i^s (Δ_i^d), with a weight for the $i = 1$ component $0 \leqslant x \leqslant 1$. A model with two isotropic gaps ($s + s$) can also not well describe the data due to the lack of a low temperature plateau as discussed previously. Meanwhile both an $s + d$ model, with one fully open gap and one line nodal gap, as well as a $d + d$ model with two nodal d-wave gaps, provide good fits to the superfluid density. The fitted parameters are $\Delta_1^s(0) = 10.12(7)$ meV, $\Delta_2^d(0) = 1.84(2)$ meV, $x = 0.70(1)$, and $T_c = 33.36(7)$ K for the $s + d$ model, while for $d + d$ they are $\Delta_1^d(0) = 1.71(3)$ meV, $\Delta_2^d(0) = 14.6(3)$ meV, $x = 0.15(1)$, and $T_c = 33.28(3)$ K. These fits yield respective zero temperature penetration depth values of $\lambda_{ab}(0) = 229.5(5)$ and 229.8(5) nm. Therefore our analysis of the superfluid density from transverse field μSR indicates the presence of multigap nodal superconductivity.

The observation of multiband nodal superconductivity in $KCa_2Fe_4As_4F_2$ is markedly different to the similar iron pnictide superconductor $CaKFe_4As_4$, where clear evidence is found for multigap nodeless superconductivity with an $s_\pm$ pairing state [12,13,33–35]. This difference is all the more puzzling since both materials are stoichiometric compounds and therefore should be similarly near optimal hole doping [32,36]. In addition, similar to many other FeAs-based superconductors but unlike the nodal material KFe_2As_2 [24], electronic structure calculations for $KCa_2Fe_4As_4F_2$ show the presence of hole pockets at the zone center and electron pockets at the edge, from which a nodeless $s_\pm$ state may be anticipated [47]. Therefore the change in gap structure between $CaKFe_4As_4$ and $KCa_2Fe_4As_4F_2$ is not likely to be analogous to the case of $(Ba_{1-x}K_x)Fe_2As_2$, where the shift from nodeless to nodal superconductivity emerges upon strong hole doping as x is increased. There is also evidence that pressure can lead to a change from nodeless to nodal superconductivity in $Ba_{0.65}Rb_{0.35}Fe_2As_2$ [48], and it was proposed that gap nodes can emerge in several iron pnictide superconductors when the height of the pnictogen above the Fe plane falls below 1.33 Å [49]. However, in $KCa_2Fe_4As_4F_2$ the As atoms are at heights of 1.40 and 1.44 Å [36], well above the proposed upper limit and even above the values found for nodeless $CaKFe_4As_4$ (1.40 and 1.35 Å) [31].

For the fits to the superfluid density of $KCa_2Fe_4As_4F_2$ using the $s + d$ and $d + d$ models, the respective magnitudes of the larger of the two gaps are $3.52(3)k_BT_c$ and $5.08(1)k_BT_c$, which we note are significantly greater than the theoretical weak coupling values ($1.76k_BT_c$ and $2.14k_BT_c$ for s- and d-wave, respectively) [50,51]. While this may suggest the presence of strongly coupled superconductivity, the fitted gap values for models with highly anisotropic gaps are sensitive to the form of the gap function and the nature of the Fermi surface. For instance, if the gap nodes are only present on a relatively small region of the Fermi surface, as was proposed for $BaFe_2(As_{0.7}P_{0.3})_2$ from ARPES measurements [52], then the superfluid density would drop less rapidly with temperature than for a d-wave gap with more extended nodal regions, which may account for the larger extracted gap values. Such a small nodal region is also consistent with the high value of T_c [52], as compared to the considerable lower value in KFe_2As_2 ($T_c \approx 3$ K). However, while in both $BaFe_2(As_{1-x}P_x)_2$ and $KCa_2Fe_4As_4F_2$ the nodal superconductivity does not arise due to tuning the carrier concentration, in $BaFe_2(As_{1-x}P_x)_2$, increasing x corresponds to doping into the Fe-As layers leading to a positive chemical pressure effect [53]. This is quite different to the case of $CaKFe_4As_4$ and $KCa_2Fe_4As_4F_2$, where the nodal superconductivity is brought about by swapping one of the spacer layers. It is noted that both these materials are asymmetric with respect to the Fe atoms, so that the As above and below the Fe planes are crystallographically inequivalent, and the effect of this asymmetry on the electronic structure and pairing symmetry requires further exploration. However, our results indicate a different route for tuning the gap structures of iron-based superconductors, which was also recently studied in the related compound $CsCa_2Fe_4As_4F_2$ [54]. As such, in order to understand this change and to identify the pairing symmetry, it is vital to further characterize the superconducting properties of $KCa_2Fe_4As_4F_2$. It is of particular importance to probe the exact nature of the gap anisotropy from single crystal studies and to look for the spin resonance via inelastic neutron scattering measurements.

This work is supported by the National Key R&D Program of China (Grant No. 2017YFA0303100) and EPSRC Grant No. EP/N023803. F.K.K.K. thanks Lincoln College, Oxford, for a doctoral studentship. D.T.A. would like to thank the Royal Society of London for support from the UK-China Newton Mobility Grant ref. IE150976.

[1] Y. Kamihara, H. Hiramatsu, M. Hirano, R. Kawamura, H. Yanagi, T. Kamiya, and H. Hosono, Iron-based layered superconductor: LaOFeP, J. Am. Chem. Soc. **128**, 10012 (2006).

[2] Y. Kamihara, T. Watanabe, M. Hirano, and H. Hosono, Iron-based layered superconductor $La[O_{1-x}F_x]FeAs$ ($x = 0.05 - 0.12$) with $T_c = 26$ K, J. Am. Chem. Soc. **130**, 3296 (2008).

[3] P. J. Hirschfeld, M. M. Korshunov, and I. I. Mazin, Gap symmetry and structure of Fe-based superconductors, Rep. Prog. Phys. **74**, 124508 (2011).

[4] I. I. Mazin, D. J. Singh, M. D. Johannes, and M. H. Du, Unconventional Superconductivity with a Sign Reversal in the Order Parameter of $LaFeAsO_{1-x}F_x$, Phys. Rev. Lett. **101**, 057003 (2008).

[5] K. Kuroki, S. Onari, R. Arita, H. Usui, Y. Tanaka, H. Kontani, and H. Aoki, Unconventional Pairing Originating from the Disconnected Fermi Surfaces of Superconducting $LaFeAsO_{1-x}F_x$, Phys. Rev. Lett. **101**, 087004 (2008).

[6] H. Ding, P. Richard, K. Nakayama, K. Sugawara, T. Arakane, Y. Sekiba, A. Takayama, S. Souma, T. Sato, T. Takahashi *et al.*, Observation of Fermi-surface–dependent nodeless superconducting gaps in $Ba_{0.6}K_{0.4}Fe_2As_2$, Europhys. Lett. **83**, 47001 (2008).

[7] R. Khasanov, D. V. Evtushinsky, A. Amato, H.-H. Klauss, H. Luetkens, Ch. Niedermayer, B. Büchner, G. L. Sun, C. T. Lin, J. T. Park, D. S. Inosov, and V. Hinkov, Two-Gap Superconductivity in $Ba_{1-x}\mathbf{K}_xFe_2As_2$: A Complementary Study of the Magnetic Penetration Depth by Muon-Spin Rotation and Angle-Resolved Photoemission, Phys. Rev. Lett. **102**, 187005 (2009).

[8] Z. Shermadini, J. Kanter, C. Baines, M. Bendele, Z. Bukowski, R. Khasanov, H.-H. Klauss, H. Luetkens, H. Maeter, G. Pascua, B. Batlogg, and A. Amato, Microscopic study of the superconducting state of the iron pnictide $RbFe_2As_2$ via muon spin rotation, Phys. Rev. B **82**, 144527 (2010).

[9] H. Kim, M. A. Tanatar, Y. J. Song, Y. S. Kwon, and R. Prozorov, Nodeless two-gap superconducting state in single crystals of the stoichiometric iron pnictide LiFeAs, Phys. Rev. B **83**, 100502 (2011).

[10] K. Nakayama, T. Sato, P. Richard, Y.-M. Xu, T. Kawahara, K. Umezawa, T. Qian, M. Neupane, G. F. Chen, H. Ding, and T. Takahashi, Universality of superconducting gaps in overdoped $Ba_{0.3}K_{0.7}Fe_2As_2$ observed by angle-resolved photoemission spectroscopy, Phys. Rev. B **83**, 020501 (2011).

[11] J.-Ph. Reid, M. A. Tanatar, X. G. Luo, H. Shakeripour, S. R. de Cotret, A. Juneau-Fecteau, J. Chang, B. Shen, H.-H. Wen, H. Kim, R. Prozorov, N. Doiron-Leyraud, and L. Taillefer, Doping evolution of the superconducting gap structure in the underdoped iron arsenide $Ba_{1-x}K_xFe_2As_2$ revealed by thermal conductivity, Phys. Rev. B **93**, 214519 (2016).

[12] K. Cho, A. Fente, S. Teknowijoyo, M. A. Tanatar, K. R. Joshi, N. M. Nusran, T. Kong, W. R. Meier, U. Kaluarachchi, I. Guillamón, H. Suderow, S. L. Bud'ko, P. C. Canfield, and R. Prozorov, Nodeless multiband superconductivity in stoichiometric single-crystalline $CaKFe_4As_4$, Phys. Rev. B **95**, 100502 (2017).

[13] P. K. Biswas, A. Iyo, Y. Yoshida, H. Eisaki, K. Kawashima, and A. D. Hillier, Signature of multigap nodeless superconductivity in $CaKFe_4As_4$, Phys. Rev. B **95**, 140505 (2017).

[14] H. Mukuda, N. Terasaki, H. Kinouchi, M. Yashima, Y. Kitaoka, S. Suzuki, S. Miyasaka, S. Tajima, K. Miyazawa, P. Shirage, H. Kito, H. Eisaki, and A. Iyo, ^{75}As-NQR/NMR studies on oxygen-deficient iron-based oxypnictide superconductors $LaFeAsO_{1-y}$ ($y = 0, 0.25, 0.4$) and $NdFeAsO_{0.6}$, J. Phys. Soc. Jpn. **77**, 093704 (2008).

[15] H.-J. Grafe, D. Paar, G. Lang, N. J. Curro, G. Behr, J. Werner, J. Hamann-Borrero, C. Hess, N. Leps, R. Klingeler, and B. Büchner, ^{75}As NMR Studies of Superconducting $LaFeAsO_{0.9}F_{0.1}$, Phys. Rev. Lett. **101**, 047003 (2008).

[16] Y. Nakai, K. Ishida, Y. Kamihara, M. Hirano, and H. Hosono, Evolution from itinerant antiferromagnet to unconventional superconductor with fluorine doping in $LaFeAs(O_{1-x}F_x)$ revealed by ^{75}As and ^{139}La nuclear magnetic resonance, J. Phys. Soc. Jpn. **77**, 073701 (2008).

[17] K. Hashimoto, M. Yamashita, S. Kasahara, Y. Senshu, N. Nakata, S. Tonegawa, K. Ikada, A. Serafin, A. Carrington, T. Terashima, H. Ikeda, T. Shibauchi, and Y. Matsuda, Line nodes in the energy gap of superconducting $BaFe_2(As_{1-x}P_x)_2$ single crystals as seen via penetration depth and thermal conductivity, Phys. Rev. B **81**, 220501 (2010).

[18] Y. Nakai, T. Iye, S. Kitagawa, K. Ishida, S. Kasahara, T. Shibauchi, Y. Matsuda, and T. Terashima, ^{31}P and ^{75}As NMR evidence for a residual density of states at zero energy in superconducting $BaFe_2(As_{0.67}P_{0.33})_2$, Phys. Rev. B **81**, 020503 (2010).

[19] M. Yamashita, Y. Senshu, T. Shibauchi, S. Kasahara, K. Hashimoto, D. Watanabe, H. Ikeda, T. Terashima, I. Vekhter, A. B. Vorontsov, and Y. Matsuda, Nodal gap structure of superconducting $BaFe_2(As_{1-x}P_x)_2$ from angle-resolved thermal conductivity in a magnetic field, Phys. Rev. B **84**, 060507 (2011).

[20] X. Qiu, S. Y. Zhou, H. Zhang, B. Y. Pan, X. C. Hong, Y. F. Dai, M. J. Eom, J. S. Kim, Z. R. Ye, Y. Zhang, D. L. Feng, and S. Y. Li, Robust Nodal Superconductivity Induced by Isovalent Doping in $Ba(Fe_{1-x}Ru_x)_2As_2$ and $BaFe_2(As_{1-x}P_x)_2$, Phys. Rev. X **2**, 011010 (2012).

[21] H. Fukazawa, Y. Yamada, K. Kondo, T. Saito, Y. Kohori, K. Kuga, Y. Matsumoto, S. Nakatsuji, H. Kito, P. M. Shirage, K. Kihou, N. Takeshita, C.-H. Lee, A. Iyo, and H. Eisaki, Possible multiple gap superconductivity with line nodes in heavily hole-doped superconductor KFe_2As_2 studied by ^{75}As nuclear quadrupole resonance and specific heat, J. Phys. Soc. Jpn **78**, 083712 (2009).

[22] J. K. Dong, S. Y. Zhou, T. Y. Guan, H. Zhang, Y. F. Dai, X. Qiu, X. F. Wang, Y. He, X. H. Chen, and S. Y. Li, Quantum Criticality and Nodal Superconductivity in the FeAs-Based Superconductor KFe_2As_2, Phys. Rev. Lett. **104**, 087005 (2010).

[23] K. Hashimoto, A. Serafin, S. Tonegawa, R. Katsumata, R. Okazaki, T. Saito, H. Fukazawa, Y. Kohori, K. Kihou, C. H. Lee, A. Iyo, H. Eisaki, H. Ikeda, Y. Matsuda, A. Carrington, and T. Shibauchi, Evidence for superconducting gap nodes in the zone-centered hole bands of KFe_2As_2 from magnetic penetration-depth measurements, Phys. Rev. B **82**, 014526 (2010).

[24] K. Okazaki, Y. Ota, Y. Kotani, W. Malaeb, Y. Ishida, T. Shimojima, T. Kiss, S. Watanabe, C.-T. Chen, K. Kihou *et al.*, Octet-line node structure of superconducting order parameter in KFe_2As_2, Science **337**, 1314 (2012).

[25] J.-P. Reid, M. A. Tanatar, A. Juneau-Fecteau, R. T. Gordon, S. R. de Cotret, N. Doiron-Leyraud, T. Saito, H. Fukazawa, Y. Kohori, K. Kihou, C. H. Lee, A. Iyo, H. Eisaki, R. Prozorov, and L. Taillefer, Universal Heat Conduction in the Iron Arsenide Superconductor KFe_2As_2: Evidence of a d-Wave State, Phys. Rev. Lett. **109**, 087001 (2012).

[26] S. Maiti, M. M. Korshunov, T. A. Maier, P. J. Hirschfeld, and A. V. Chubukov, Evolution of the Superconducting State of Fe-Based Compounds with Doping, Phys. Rev. Lett. **107**, 147002 (2011).

[27] R. Thomale, C. Platt, W. Hanke, J. Hu, and B. A. Bernevig, Exotic d-Wave Superconducting State of Strongly Hole-Doped $\mathbf{K}_xBa_{1-x}Fe_2As_2$, Phys. Rev. Lett. **107**, 117001 (2011).

[28] W.-C. Lee, S.-C. Zhang, and C. Wu, Pairing State With a Time-Reversal Symmetry Breaking in FeAs-Based Superconductors, Phys. Rev. Lett. **102**, 217002 (2009).

[29] Z. Lotfi Mahyari, A. Cannell, C. Gomez, S. Tezok, A. Zelati, E. V. L. de Mello, J.-Q. Yan, D. G. Mandrus, and J. E. Sonier,

Zero-field μSR search for a time-reversal-symmetry-breaking mixed pairing state in superconducting $Ba_{1-x}K_xFe_2As_2$, Phys. Rev. B **89**, 020502 (2014).

[30] V. Grinenko, P. Materne, R. Sarkar, H. Luetkens, K. Kihou, C. H. Lee, S. Akhmadaliev, D. V. Efremov, S.-L. Drechsler, and H.-H. Klauss, Superconductivity with broken time-reversal symmetry in ion-irradiated $\mathbf{Ba_{0.27}K_{0.73}Fe_2As_2}$ single crystals, Phys. Rev. B **95**, 214511 (2017).

[31] A. Iyo, K. Kawashima, T. Kinjo, T. Nishio, S. Ishida, H. Fujihisa, Y. Gotoh, K. Kihou, H. Eisaki, and Y. Yoshida, New-structure-type Fe-based superconductors: $CaAFe_4As_4$ (A = K, Rb, Cs) and $SrAFe_4As_4$ (A = Rb, Cs), J. Am. Chem. Soc. **138**, 3410 (2016).

[32] W. R. Meier, T. Kong, U. S. Kaluarachchi, V. Taufour, N. H. Jo, G. Drachuck, A. E. Böhmer, S. M. Saunders, A. Sapkota, A. Kreyssig, M. A. Tanatar, R. Prozorov, A. I. Goldman, F. F. Balakirev, A. Gurevich, S. L. Bud'ko, and P. C. Canfield, Anisotropic thermodynamic and transport properties of single-crystalline $CaKFe_4As_4$, Phys. Rev. B **94**, 064501 (2016).

[33] D. Mou, T. Kong, W. R. Meier, F. Lochner, L.-L. Wang, Q. Lin, Y. Wu, S. L. Bud'ko, I. Eremin, D. D. Johnson, P. C. Canfield, and A. Kaminski, Enhancement of the Superconducting Gap by Nesting in $CaKFe_4As_4$: A New High Temperature Superconductor, Phys. Rev. Lett. **117**, 277001 (2016).

[34] K. Iida, M. Ishikado, Y. Nagai, H. Yoshida, A. D. Christianson, N. Murai, K. Kawashima, Y. Yoshida, H. Eisaki, and A. Iyo, Spin resonance in the new-structure-type iron-based superconductor $CaKFe_4As_4$, J. Phys. Soc. Jpn. **86**, 093703 (2017).

[35] J. Cui, Q.-P. Ding, W. R. Meier, A. E. Böhmer, T. Kong, V. Borisov, Y. Lee, S. L. Bud'ko, R. Valentí, P. C. Canfield, and Y. Furukawa, Magnetic fluctuations and superconducting properties of $CaKFe_4As_4$ studied by ^{75}As NMR, Phys. Rev. B **96**, 104512 (2017).

[36] Z.-C. Wang, C.-Y. He, S.-Q. Wu, Z.-T. Tang, Y. Liu, A. Ablimit, C.-M. Feng, and G.-H. Cao, Superconductivity in $KCa_2Fe_4As_4F_2$ with separate double Fe_2As_2 layers, J. Am. Chem. Soc. **138**, 7856 (2016).

[37] Z. Wang, C. He, Z. Tang, S. Wu, and G. Cao, Crystal structure and superconductivity at about 30 K in $ACa_2Fe_4As_4F_2$ (A = Rb, Cs), Sci. China Mater. **60**, 83 (2017).

[38] P. J. C. King, R. de Renzi, S. P. Cottrell, A. D. Hillier, and S. F. J. Cox, ISIS muons for materials and molecular science studies, Phys. Scr. **88**, 068502 (2013).

[39] F. L. Pratt, WIMDA: a muon data analysis program for the Windows PC, Physica B: Condensed Matter **289-290**, 710 (2000).

[40] R. P. Singh, A. D. Hillier, B. Mazidian, J. Quintanilla, J. F. Annett, D. M. Paul, G. Balakrishnan, and M. R. Lees, Detection of Time-Reversal Symmetry Breaking in the Noncentrosymmetric Superconductor Re_6Zr Using Muon-Spin Spectroscopy, Phys. Rev. Lett. **112**, 107002 (2014).

[41] D. T. Adroja, A. Bhattacharyya, M. Telling, Y. Feng, M. Smidman, B. Pan, J. Zhao, A. D. Hillier, F. L. Pratt, and A. M. Strydom, Superconducting ground state of quasi-one-dimensional $K_2Cr_3As_3$ investigated using μSR measurements, Phys. Rev. B **92**, 134505 (2015).

[42] E. H. Brandt, Muon spin rotation and the vortex lattice in superconductors, Physica B: Condensed Matter **404**, 695 (2009).

[43] E. H. Brandt, Properties of the ideal Ginzburg-Landau vortex lattice, Phys. Rev. B **68**, 054506 (2003).

[44] V. I. Fesenko, V. N. Gorbunov, and V. P. Smilga, Analytical properties of muon polarization spectra in type-II superconductors and experimental data interpretation for mono- and polycrystalline HTSCs, Physica C: Superconductivity **176**, 551 (1991).

[45] B. S. Chandrasekhar and D. Einzel, The superconducting penetration depth from the semiclassical model, Ann. Phys. **505**, 535 (1993).

[46] A. Carrington and F. Manzano, Magnetic penetration depth of MgB_2, Physica C **385**, 205 (2003).

[47] G. Wang, Z. Wang, and X. Shi, Self-hole-doping-induced superconductivity in $KCa_2Fe_4As_4F_2$, Europhys. Lett. **116**, 37003 (2016).

[48] Z. Guguchia, A. Amato, J. Kang, H. Luetkens, P. K. Biswas, G. Prando, F. von Rohr, Z. Bukowski, A. Shengelaya, H. Keller *et al.*, Direct evidence for a pressure-induced nodal superconducting gap in the $Ba_{0.65}Rb_{0.35}Fe_2As_2$ superconductor, Nat. Commun. **6**, 8863 (2015).

[49] K. Hashimoto, S. Kasahara, R. Katsumata, Y. Mizukami, M. Yamashita, H. Ikeda, T. Terashima, A. Carrington, Y. Matsuda, and T. Shibauchi, Nodal Versus Nodeless Behaviors of the Order Parameters of LiFeP and LiFeAs Superconductors from Magnetic Penetration-Depth Measurements, Phys. Rev. Lett. **108**, 047003 (2012).

[50] J. Bardeen, L. N. Cooper, and J. R. Schrieffer, Microscopic theory of superconductivity, Phys. Rev. **106**, 162 (1957).

[51] H. Won and K. Maki, d-wave superconductor as a model of high-T_c superconductors, Phys. Rev. B **49**, 1397 (1994).

[52] Y. Zhang, Z. R. Ye, Q. Q. Ge, F. Chen, J. Jiang, M. Xu, B. P. Xie, and D. L. Feng, Nodal superconducting-gap structure in ferropnictide superconductor $BaFe_2(As_{0.7}P_{0.3})_2$, Nat. Phys. **8**, 371 (2012).

[53] S. Jiang, H. Xing, G. Xuan, C. Wang, Z. Ren, C. Feng, J. Dai, Z. Xu, and G. Cao, Superconductivity up to 30 K in the vicinity of the quantum critical point in $BaFe_2(As_{1-x}P_x)_2$, J. Phys.: Condens. Matter **21**, 382203 (2009).

[54] F. K. K. Kirschner, D. T. Adroja, Z. C. Wang, F. Lang, M. Smidman, P. J. Baker, G.-H. Cao, and S. J. Blundell, Two-gap superconductivity with line nodes in $CsCa_2Fe_4As_4F_2$, Phys. Rev. B **97**, 060506(R) (2018).